Available online at www.sciencedirect.com
ScienceDirect
Trans. Nonferrous Met. Soc. China 23(2013) 1480−1488
Transactions of Nonferrous Metals Society of China
www.tnmsc.cn

Technological mineralogy and environmental activity of zinc leaching residue from zinc hydrometallurgical process

Mi LI, Bing PENG, Li-yuan CHAI, Ning PENG, Xian-de XIE, Huan YAN

School of Metallurgy and Environment, Central South University, Changsha 410083, China

Received 15 March 2012; accepted 30 October 2012

Abstract: Chemical, physical, structural and morphological properties of zinc leaching residue were examined by the combination of various detection means such as AAS, XRF, XRD, Mössbauer spectrometry, SEM−EDS, TG−DSC, XPS and FTIR. The toxicity characteristic leaching procedure (TCLP) was used to investigate the environmental activity of zinc leaching residue for a short contact time. The phase composition analysis indicated that the zinc leaching residue mainly consists of super refined flocculent particles including zinc ferrite, sulfate and silicate. The physical structural analysis showed that it has a thermal instability and strong water absorption properties. The results of TCLP indicated that the amounts of Zn and Cd in the leaching solution exceed 40 and 90 times of limit, respectively, which demonstrate that this residue is unstable in weak acidic environment for a short contact time.
Key words: zinc leaching residue; phase composition; microstructure; technological mineralogy; leaching toxicity

1 Introduction

Zinc leaching residue (ZLR) generated in traditional zinc hydrometallurgical process is classified as a hazardous intermediate due to its potential leaching of toxic metal ions such as Zn, Pb, Cd and As [1−3]. At present, the sludge is mainly stockpiled for future treatment or as a secondary resource for recovery of metal values [4]. The huge quantities of these residues result in wasting metal values and environmental pollution due to the heavy metal content. Waelz kiln processing [5] and hot acid leaching [6] routes are usually used for treating this sludge. During Waelz kiln processing, the iron is reduced to metallic phase which makes the recovery of iron difficult. In hot acid leaching process, a complicated iron precipitation process is needed. Furthermore, many other pyrometallurgical and hydrometallurgical methods such as alkaline leaching [7], caustic leaching [8] and transformation roasting [9,10], have been developed to dispose this sludge. The choice between hydrometallurgical or pyrometallurgical processing routes strongly depended on the sludge characteristics, including the number of valuable elements, mineralogical phase composition, leachable and thermal decomposition properties. Therefore, a detailed and complicated understanding of the characterization of ZLR becomes an important tool for defining the most appropriate recycling strategy.

During the past decades, a considerable quantity of solid wastes have been investigated systematically by many researchers and plenty of valuable data were obtained successfully, such as the ferrous slag [11] as well as the last incineration slag [12]. However, some critical technological mineralogy information of ZLR is still unclear, especially for the phase composition, thermal properties and grain distributions features of the main elements of zinc and iron that exist in sludge, except a small number of literatures were reported [3]. The lacking of basic knowledge on ZLR can necessarily lead to difficulties in separating zinc and iron in traditional zinc hydrometallurgy process which can eventually result in substantial stockpile of ZLR in great abundance in an inevitable way and a magnitude of metal values left to be unrecovered.

The purpose of this research is to determine the mineralogy characterizations of ZLR collected from a zinc hydrometallurgy plant in China, including chemical composition, phase composition, microstructure, thermal properties and leaching toxicity. Most significantly, the

Foundation item: Project (2011AA061001) supported by the Hi-Tech Research and Development Program of China; Project (50830301) supported by the Key Program of National Natural Science Foundation of China; Project (50925417) supported by the National Science Fund for Distinguished Young Scientists of China
Corresponding author: Bing PENG; Tel: +86-731-88830875; E-mail: pb1956@yahoo.cn
DOI: 10.1016/S1003-6326(13)62620-5

research can provide information to develop new technology for the achievement of separating iron and zinc from ZLR.

2 Experimental

A sample of zinc ferrite sludge was obtained from a zinc hydrometallurgy plant in China. This sludge was produced during the oxidative roasting and leaching of zinc concentrates. In this study, all samples were dried at 105 °C for 3 h and stored above silica gel in a desiccator. Some parts of residues were milled in an XZM-100 vibration grinding mill for 3 min to get the powders suitable for XRF, XRD, TG-DSC, FTIR, XPS, Mössbauer and chemical analyses, and unground samples were used for SEM−EDS analysis directly.

The leaching toxicity characteristic of heavy metals in ZLR was determined by TCLP (USEPA method 1311) [13]. The three-stage BCR sequential extraction procedure was employed to investigate the environmental activity of heavy metals. The different solvents, extraction liquids and conditions taken during the extraction procedure are shown in Table 1 [14,15]. The potential toxic content in solution was analyzed by atomic absorption spectrometry (AAS) using the flame technique (SUPER, TAS−990).

The chemical composition of ZLR was detected firstly by XRF (Rigaku, model ZSX Primus II) and then the main metal elements such as iron, zinc, calcium, lead, manganese, copper and magnesium were analyzed by AAS based to XRF results. The sample was prepared by dissolution in an acid admixture for the determination of metal content by using AAS.

Table 1 BCR three-stage sequential extraction scheme

Stage	Fraction	Reagent in 1 g sample	Condition
1	Acid exchangeable form	40 mL CH_3COOH (0.11 mol/L)	16 h at room temperature
2	Reducible form	40 mL $NH_2OH·HCl$ (0.11 mol/L, pH=2 adjusted with HNO_3)	16 h at room temperature
3	Oxidizable form	10 mL H_2O_2 (8.8 mol/L, pH=2 adjusted with HNO_3)	1 h at (85±2) °C
		10 mL H_2O_2 (8.8 mol/L, pH=2 adjusted with HNO_3)	1 h at (85±2) °C
		50 mL CH_3COONH_4 (1 mol/L, pH=2 adjusted with HNO_3)	1 h at room temperature
4	Residual form*	Aqua regia	

*Digestion of the residual material is not a specification of the BCR protocol.

The phase composition of zinc was investigated using chemical analysis after dissolving sample in different solvents. During the analysis, one main phase was dissolved in one specific solvent. The leachate was filtrated with vacuum filter after dissolving completely. The filtration residues were used for next phase analysis while the supernate was analyzed by AAS to examine the content. All analysis processes are listed in Fig. 1 [16].

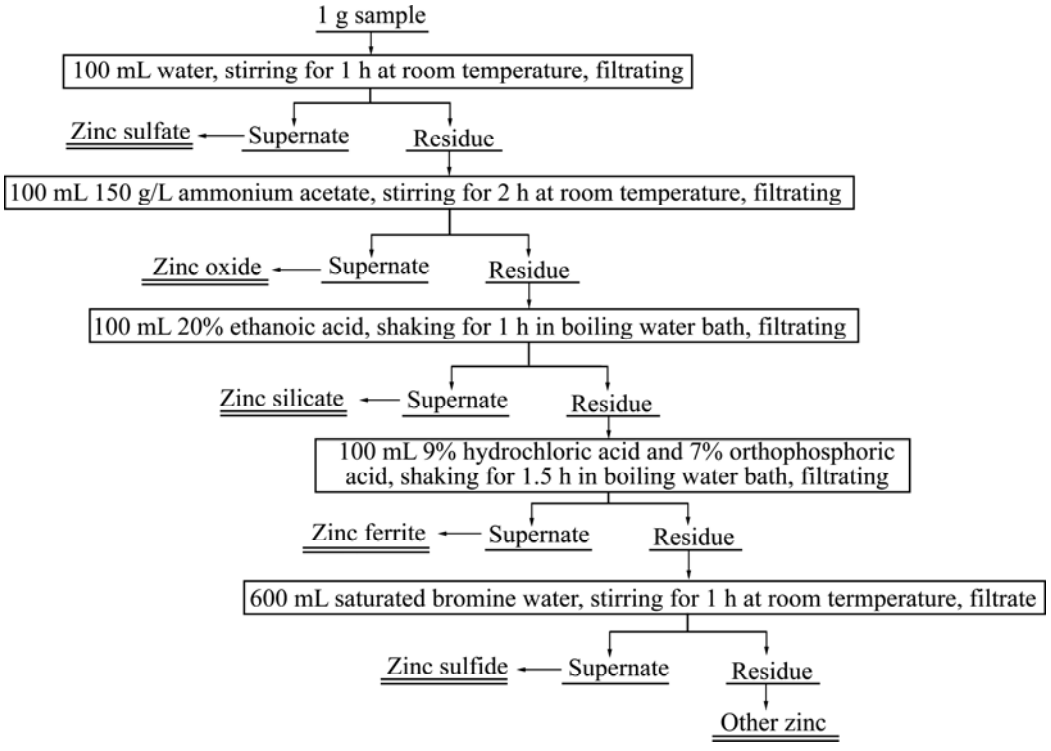

Fig. 1 Methodology used for chemical phase analysis of zinc leaching residue

The phases present in ZLR were detected by XRD (Rigaku, TTR-III). XRD patterns of the sample were obtained with monochromated Cu K_α radiation in 2θ ranging from 10° to 80° with scan step of 0.05°. The patterns were analyzed by using JADE 5.0 X-pert software. The phase composition of iron was investigated by Mössbauer spectra in a standard spectrometer at constant acceleration and room temperature. A 70 mCi ^{57}Co(Gr) source was taken and the isomer shifts were given relative to α-Fe. The spectra obtained in the experiments were analyzed using a standard software based on the least-squares method. The parameters of hyperfine interactions such as isomer shift (IS), quadrupole splitting (QS) and effective internal magnetic field (H_{eff}) were determined. The relative shares (area, %) of different spectrum components were determined on the intensities of the corresponding lines. The identification of various phases was based on the data from references [17].

SEM (JEOL, JSM-6360LV) and EDS (EDAX, EDX-GENESIS 60S) were used to gain further information of ZLR structure, morphology and special part chemical composition. The same sample was also subjected to the element distribution analysis through X-ray mapping analysis via SEM.

Simultaneous TG-DSC investigation was carried out in a thermal analyzer (NETZSCH STA 449C). A sample weighing between 10 mg and 15 mg was placed in a 1 mL aluminum crucible and heated at a rate of 10 °C/min from room temperature up to 1300 °C under an argon flux of 50 mL/min.

The grain morphology and mineralogical surface composition of ZLR were examined by XPS (Kratos Ltd, XSAM800) with Mg K_α X-ray source in a vacuum of 10^{-6} Pa.

FTIR spectra were collected with a Fourier infrared spectrometer (Nicolet, IS10) on KBr pellets in the range of 4000 and 400 cm^{-1} with 4 cm^{-1} resolution and 32 scans to study the molecular bonding structure and conform the phase composition.

3 Results and discussion

3.1 Chemical compositions of zinc leaching residue

The elemental composition of ZLR sample analyzed by XRF and AAS are given in Tables 2 and 3, respectively. The data from AAS are similar to those from XRF. Fe, Zn, S, Si and Pb are the major elements in ZLR. In addition, the results revealed that there are high contents of Mn, Ca, Al and Cu in the sludge. The chemical composition of ZLR mainly depends on the content of impurity elements in zinc concentrate, the type of zinc produced and the particular operations performed during zinc production such as oxidizing roasting and methods used for dehydration of leaching sludge.

Table 2 Chemical composition of zinc leaching residue obtained by XRF (mass fraction, %)

Fe	Zn	S	Si	Pb	Ca
23.91	19.7	6.40	4.47	4.35	2.20
Mn	Al	Cu	As	Cr	Cd
1.53	1.15	0.80	0.52	0.017	0.31
Mg	K	0.24	Sr	Sn	
0.26	Ba	0.204	0.162	0.162	
Bi	Ni	Ti	P	Ag	
0.131	0.011	0.0566	0.043	0.037	

Table 3 Chemical composition of zinc leaching residue obtained by chemical analysis (mass fraction, %)

Fe	Zn	Ca	Pb	Mn	Cu	Mg
24.02	19.57	1.97	4.18	1.41	0.91	0.37

Figure 2 shows the XRD pattern of ZLR. It is seen from Fig. 2 that the zinc mainly presents in the phases of zinc ferrite ($ZnFe_2O_4$), zinc silicate (Zn_2SiO_4), zinc sulfide (ZnS), zinc oxide (ZnO), and zinc sulfate ($ZnSO_4$). The chemical approach was applied to determining the content of each phase, and the results are given in Table 4.

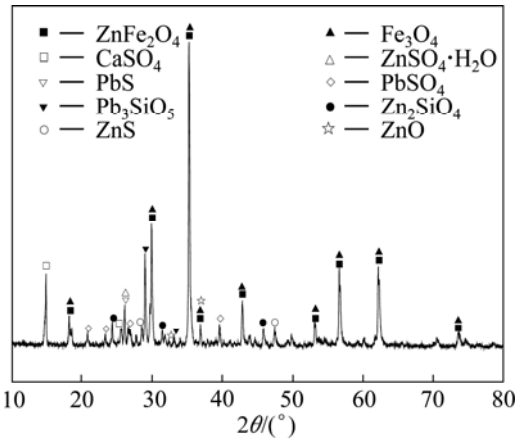

Fig. 2 XRD pattern of zinc leaching residue

Table 4 Phase composition of zinc in zinc leaching residue obtained by chemical analysis

Phase	w(Zn)/%	Phase occupation ratio/%
$ZnSO_4$	4.47	22.86
ZnO	1.34	6.87
Zn_2SiO_4	0.97	4.98
$ZnFe_2O_4$	10.92	55.72
ZnS	1.82	9.3
Others	0.05	0.2
Total	19.57	100

The zinc ferrite and zinc silicate are usually formed in the process of oxidation roasting of zinc sulfide concentrate, and the main reactions are listed in reactions (1) and (2). The zinc sulfide comes from the unreacted zinc concentrate in zinc calcine, and this phase is mainly present in the inner part of the particles with the surface wrapped by zinc ferrite according to Ref. [18]

$$ZnO+Fe_2O_3=ZnFe_2O_4 \quad (1)$$

$$2ZnO+SiO_2=Zn_2SiO_4 \quad (2)$$

The element lead exists in the forms of PbS, Pb_3SiO_5 and $PbSO_4$. During oxidation roasting process, most PbS is changed into PbO and then reacts with SiO_2 to form Pb_3SiO_5 at high temperature or reacts with sulfuric acid in leaching process to form insoluble $PbSO_4$. However, the phase of Fe_3O_4 is not assured in the sample according to XRD because the patterns from $ZnFe_2O_4$ and Fe_3O_4 are overlapped at all peaks. Thus, in order to improve the phase identification in ZLR samples, it is necessary to use other techniques like, Mössbauer spectroscopy, SEM with EDS and X-ray mapping analysis.

As for confirmation of Fe ions oxidation state, the Mössbauer spectrum at room temperature for ZLR is displayed in Fig. 3. The hyperfine field (H_{eff}), isomer shift (*IS*), quadrupole splitting (QS) and half line width ($\Gamma/2$) obtained from the best fitted Mössbauer spectrum line are presented in Table 5. It is observed that only one petronas line is detected by Mössbauer spectrum fitted by the least-square method in Fig. 3. This indicates that the iron exists mainly in the form of zinc ferrite in ZLR. The ferriferous oxide may not exist in ZLR or the content of this phase is lower than the detection limit of the Mössbauer analyzer (below 2%). Thus, the content of ferriferous oxide could be neglected when developing new methods for recovering metals from ZLR. The values obtained for $ZnFe_2O_4$ are in agreement with those reported in Res. [19,20].

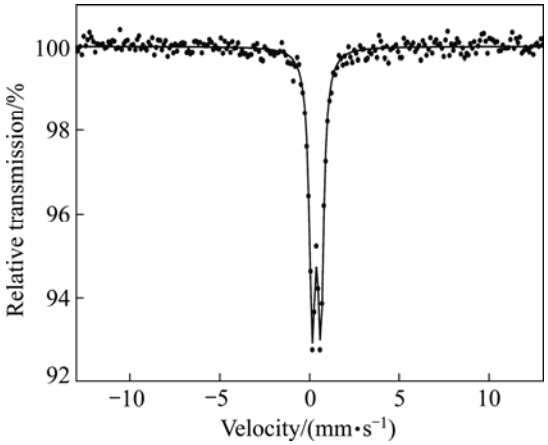

Fig 3 Mössbauer spectrum of zinc leaching residue

Table 5 Mössbauer data of zinc leaching residue

Phase	H_{eff}/ (A·m^{-1})	*IS*/ (mm·s^{-1})	QS/ (mm·s^{-1})	$\Gamma/2$/ (mm·s^{-1})	Area/ %
$ZnFe_2O_4$	−	0.39	0.47	0.2	100

3.2 Structural feature

Scanning electron microstructural analysis of ZLR was carried out and the results are shown in Figs. 4 and 5. Based on these microphotographs and EDS, it can be seen that the phase composition and the particle size of ZLR are not homogeneous. Figure 4 shows the general ZLR particles in spherical and irregular bulk shapes. The biggest particle is about 10 μm and the smallest one below 1 μm. The agglomerated morphology is predominant with super fine independent particles or covers on the surface of larger spherical particles, which appear in the oxidation roasting process of zinc concentrate. CHEN and DUTRIZAC [21] studied the mineralogical changes during roasting of zinc sulfide and found that zinc ferrite was generated inevitably and existed on the surface of un-reacted zinc sulfide core, which would hinder the zinc sulfide to convert into zinc oxide. During acid leaching, most of exposed zinc oxide is dissolved with the unleachable metals such as $PbSO_4$, $CaSO_4$, $ZnSiO_4$, ZnS, PbS and the ZnO encapsulated by $ZnFe_2O_4$ left in ZLR. Fortunately, the zinc ferrite

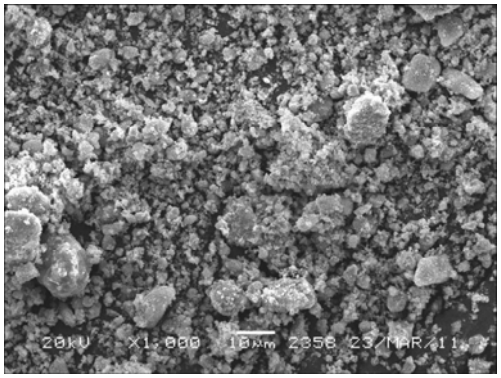

Fig. 4 SEM image of zinc leaching residue

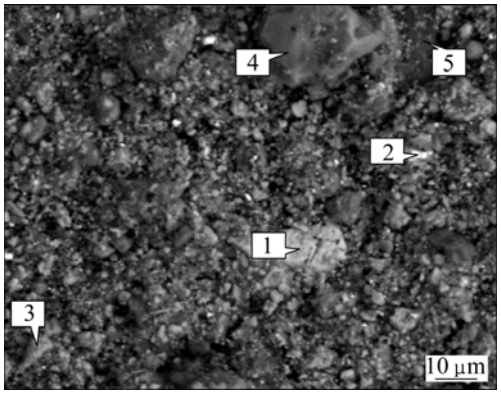

Fig. 5 Back scattered electron image of zinc leaching residue

produced in roasting process is in a porous structure and the acid could pass through the zinc ferrite layer to achieve the inner part of the zinc oxide and dissolve the zinc oxide under mechanical agitation. Thus, the zinc ferrite disabsorpted from the zinc sulfide core is in floccus shape and forms predominant features observed in the SEM image. Figure 5 shows a typical phase distribution of ZLR and Table 6 shows the results of EDS analysis of the selected areas in Fig. 5. Based on EDS analysis, the phases of Pb, S and O as major elements in highlight area 2 are assigned to lead sulfate or lead sulfide, which is consistent with the results of XRD analysis. Zn and S as major elements in area 1 are assigned to zinc sulfide, which was also identified by other researches [22]. The light grey area 3 is rich in Fe, Zn and O, where the zinc ferrite is present. This phase possesses the agglomeration structure and super fine particle size with the diameter varying from 1 μm to 20 μm. In addition, this phase is also in the form of spherical shape with light grey color in the backscatter electronic photos. Area 4 shows a large dark area with the predominant elements of Mn, O and S, showing the existence of $MnSO_4$, which is not observed by XRD due to the lower content of Mn in the ZLR. Area 5 is rich in Ca, S and O, which proves the presence of $CaSO_4$.

Table 6 EDS results of areas in Fig. 5

Element	Mole fraction/%				
	Area 1	Area 2	Area 3	Area 4	Area 5
Zn	58.1	5.42	23.49	7.79	7.31
Fe	5.67	3.75	32.89	11.49	10.36
O	6.22	6.56	17.98	13.08	21.09
S	29.03	8.47	3.04	2.72	27.85
Si	0.98	2.05	3.35	−	1.68
K	−	−	−	2.93	−
Ca	−	−	0.95	−	31.71
Pb	−	69.83	12.99	7.77	−
Cu	−	3.92	−	2.49	−
Mn	−	−	1.38	39.94	−
Cr	−	−	2.92	−	−
Al	−	−	1.01	−	−
As	−	−	−	11.78	−

In order to understand the main elements distribution in ZLR, a secondary electron scanning image and the X-ray mappings for the elements of Fe, Zn, S, O, Si and Ca were undertaken and the results are given in Fig. 6. Figure 6 indicates that the elements of Fe, Zn and O are in the forms of zinc ferrite or iron oxide, but

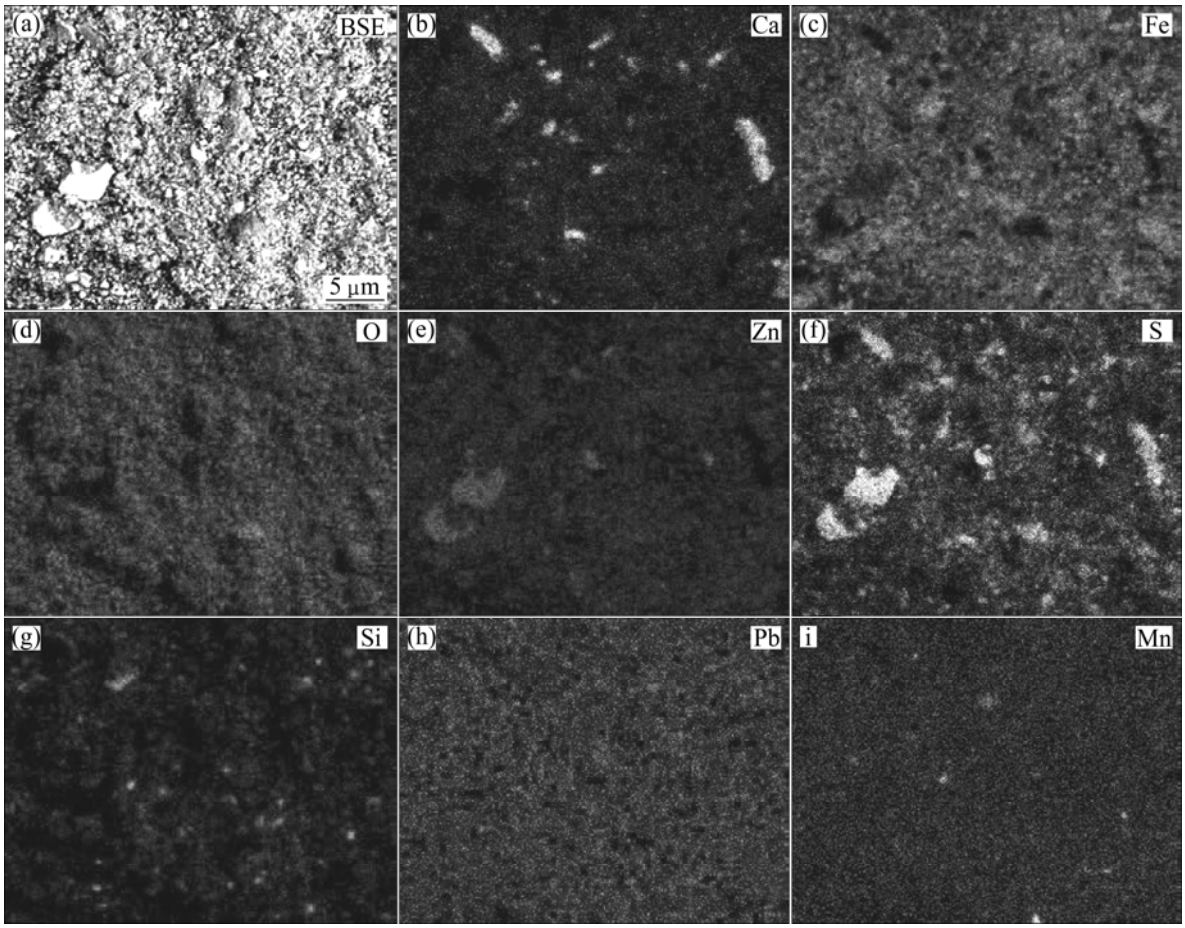

Fig. 6 Backscattered electron image (a) and elements (b, c, d, e, f, g, h, i) distribution of zinc leaching residue

the Mössbauer analysis did not detect the presence of iron oxide. On the other hand, some areas without iron but rich in zinc and sulfur are observed, which suggests the presence of zinc sulfide. Calcium appears with high amount in regions with a long bar-type shape and large size where iron is not present. In this area, sulfur element also occurrs. Probably, it is a phase containing calcium, sulfur and oxygen originated from the zinc concentrates used in zinc production. Besides, calcium also distributes with lower concentration in regions where other elements such as iron, zinc and silicate are present, which can suggest the presence of micro amount of gangue. Lead disperses in ZLR homogeneously, indicating that the lead-containing phases emerges in the super fine particles, and other phase particles might be packed by this feature. Manganese might exist in the form of $MnSO_4$ or MnO_2; however, it is not detected by XRD due to its insufficient amount for an appropriate detection.

3.3 Thermal properties

TG−DSC analysis was conducted to check thermal decomposition properties of ZLR and the result is shown in Fig. 7.

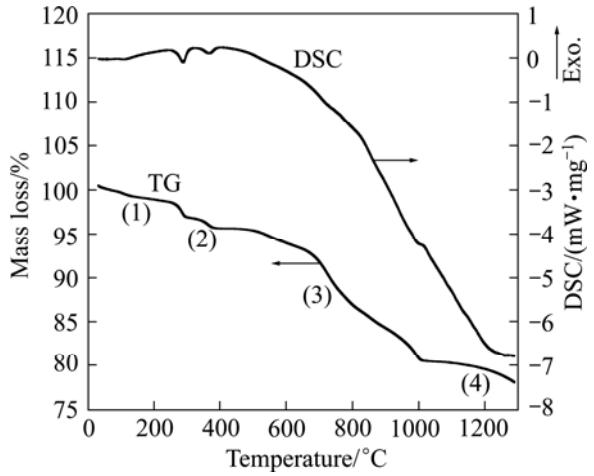

Fig. 7 TG−DSC curves of zinc leaching residue

The TG curve shows four degradation stages during heating from room temperature to 1300 °C. The initial mass loss of 1.5% (1) by the release of adsorbed water from $ZnSO_4{\cdot}nH_2O$ and $CaSO_4{\cdot}nH_2O$ was observed from 100 °C to 200 °C [23]. A mass loss of 3.42% (2) appears in the temperature ranging from 200 °C to 400 °C with two sub-steps by small endothermic peaks of DSC curve, which indicates several dehydration reactions occurring simultaneously [24]. The third temperature region appears in 700−1000 °C as a sharp decrease of mass (3) for sulfate decomposition and release of sulfur trioxide. Combined with TG curve and XRD analysis, it is concluded that the $ZnSO_4$ decomposes from 700 °C to 860 °C, $PbSO_4$ does from 759 °C to 1000 °C and $MnSO_4$ does from 750 °C to 950 °C [25,26]. The total mass loss by sulfur trioxide observed during thermal decomposition process is approximately 15%, which is consistent with the sulfur content detected by a chemical analyses in Table 2 and Table 3. The last mass loss (4) temperature region by oxides decomposition and oxides volatile is from 1000 °C to 1300 °C. The primary reactions occurring in the decomposition of ZLR are listed in formula (3)−(7).

$$ZnSO_4{\cdot}nH_2O = ZnSO_4 + nH_2O \quad (3)$$

$$CaSO_4{\cdot}nH_2O = CaSO_4 + nH_2O \quad (4)$$

$$ZnSO_4 = ZnO + SO_3 \quad (5)$$

$$3MnSO_4 = Mn_3O_4 + SO_2 + 2SO_3 \quad (6)$$

$$PbSO_4 = PbO + SO_3 \quad (7)$$

It is concluded that most sulfur is removed as SO_3 at temperature above 700 °C according to the results of TG−DSC analysis. It is necessary to use a specific device to prevent the sulfur oxide from escaping into atmosphere, or utilize additive reagent to fix the sulfur when pyrometallurgical routes are used to treat this sludge.

3.4 Surface performance

It is very important to investigate the surface performance of ZLR due to the fact that most solid waste treatments are initially controlled by surface chemical reactions. XPS analysis was conducted to command elemental composition and oxidation states on the surface. The spectra of Fe 2p, Zn 2p, S 2p and Pb 4f peaks are displayed in Fig. 8, respectively. The particle surface exhibits the multi-elemental chemicals with complex elemental composition. The iron spectrum in Fig. 8(a) with the binding energies of Fe $2p_{3/2}$ and Fe $2p_{1/2}$ are measured as 711.1 eV and 724.8 eV, respectively, which indicates the presence of $ZnFe_2O_4$ [27]. Figures 8(b), (c) and (d) show Zn 2p, S 2p and Pb 4f peak separations. XPS data used in the peak separations were obtained from previous researches [28,29]. These peak separations indicate that the particle surface of ZLR is wrapped by $ZnSO_4$, ZnO, $CaSO_4$, and $ZnFe_2O_4$. The sulfide identified by XRD and SEM analyses is not detected on the surface by XPS, which means that sulfide presents in the core of the particles. The element sulfur exists in sulfate such as $CaSO_4$ and $ZnSO_4$ on the surface, which is detected by TG−DSC.

3.5 Molecular bonding structure

The infrared spectrum of ZLR is given in Fig. 9. The spectrum displays at 3400 cm^{-1} for the O—H stretching of hydrogen bonded water (H—O), 1620 cm^{-1} for the vibration of water molecule (H_2O) [11]. Two

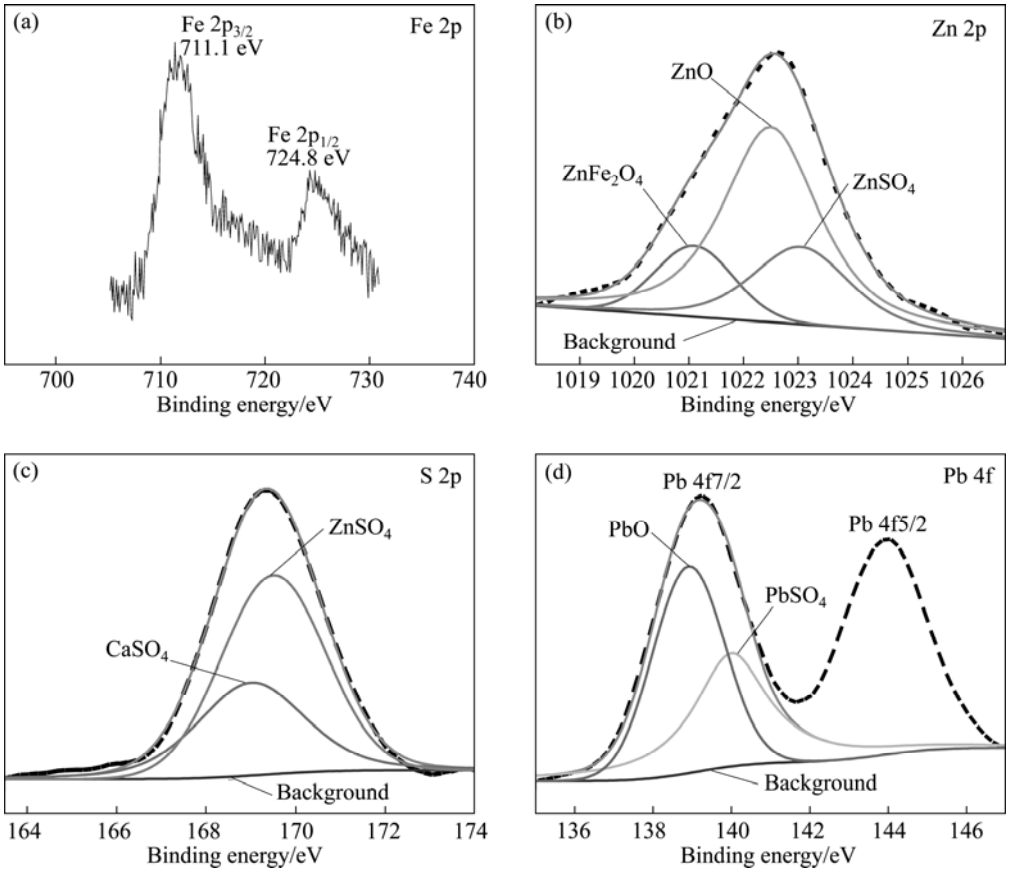

Fig. 8 X-ray photoelectron spectra of Fe 2p (a), Zn 2p (b), S 2p (c) and Pb 4f (d)

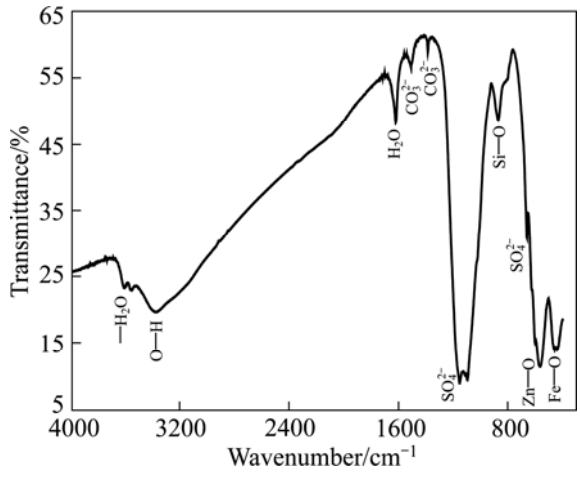

Fig. 9 FTIR spectrum of zinc leaching residue prepared with KBr pellets

strong characteristic absorption peaks are located at 560 cm^{-1} and 420 cm^{-1} for the stretching vibrations of Zn—O bonds in tetrahedral positions and Fe—O bonds in octahedral positions, respectively [30], which indicates the existence of simple oxide and spines such as ZnO and $ZnFe_2O_4$. The bands near 3550 cm^{-1} and 3600 cm^{-1} are assigned to crystal water (H_2O) attached to $CaSO_4$ and $ZnSO_4$, which are also observed in TG−DSC analysis. The strong bands located around 1100 cm^{-1} and 1160 cm^{-1} are sulfate (SO_4^{2-}) vibration and the other sulfate bands are obtained around 660 cm^{-1} [11]. A weak band at 870 cm^{-1} is assigned to Si—O vibrations for Pb_3SiO_5 and Zn_2SiO_4 observed by XRD. It is seen from the infrared spectra that the bands of CO_3^{2-} vibration around 1380 cm^{-1} and 1500 cm^{-1} are detected [30]. However, the carbonate is not observed from other analysis due to its lower content in ZLR.

It is concluded from the above analysis of infrared spectra that crystal water, sulfate and zinc ferrite with the strongest vibration band are the main phases present in ZLR. A strong trend of water absorption is due to the existence of $ZnSO_4$ and $CaSO_4$. So ZLR should be stored in a dry condition in the case that moisture leads to the dissolution of heavy metal ions such as Pb, Cd, Zn and As.

3.6 Leaching toxicity and environmental activity

The TCLP results are shown in Table 7. The concentrations of Zn, Pb, Cd, As and Ni are 4589, 1.4, 93.5, 0.L and 0.2 mg/L, respectively. The results show that the solubilization of Zn in the sludge is 40 times higher than that of Chinese regulatory limit 100 mg/L, and that of Cd is 90 times higher than that of USEPA regulatory limit 1.0 mg/L in a weak acidic environment [31].

Table 7 TCLP test results for zinc leaching residue (mg/L)

Element	TCLP	Regulatory threshold (USEPA)	Regulatory threshold (China)
Zn	4589	−	100
Pb	1.4	5.0	5.0
Hg	ND	0.2	0.1
Se	ND	1.0	1.0
Cd	93.5	1.0	1.0
As	0.3	5.0	5.0
Ni	0.2	−	5.0
Cr	ND	5.0	5.0

*ND, not detected. The detection limit is 0.1 mg/L for Se, Cr and 0.01 mg/L for Hg.

The distributions of heavy metals in different phases extracted according to BCR fractionation scheme are shown in Fig. 10. The ranking of metals in different BCR fractions according to their contribution is Cd>Zn>Cu> Pb in soluble forms, Pb>Cu>Cd>Zn in reducible fraction, Cu>Cd>Pb>Zn in oxidisable fraction and Cu>Pb> Zn>Cd in residual fraction. The main proportion of zinc (about 19.57%) in ZLR was found in soluble fraction, which indicates that zinc occurs in exchangeable forms such as $ZnSO_4$ conformed by XRD and XPS. High toxicity element of Cd (about 33.2%) could be easily released to groundwater in weak acidic environment. About 20.96% of Pb exists in the reducible form equal to combination patterns of Fe−Mn oxide [32]. The Pb combined with ionic form in amorphous and crystalline Fe−Mn oxide might release to water and soil due to the break of ionic bond in long-term storage. Zn, Pb and Cd distribute almost equally in the oxidisable form (9%−10%) coinciding with organic and sulfur compounds. Cu also shows considerable fraction oxidisable forms. All heavy metals might be converted into the high migration form of sulfate under acid biological oxidation conditions and endanger the environment with the existence of a large number of sulfur compounds [33]. Metals in residual fraction associated mainly with insoluble minerals are difficult to be released to water, and this part is expected to exist stably for a long time in environment.

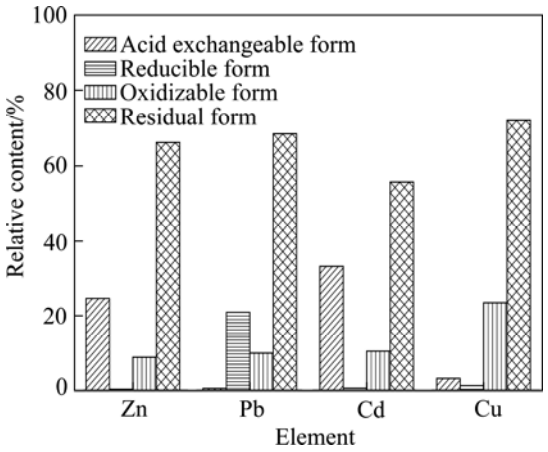

Fig. 10 Chemical fraction of heavy metals in sludge by BCR procedure

4 Conclusions

1) The mineralogical analysis indicated that the residue is primarily composed of $ZnFe_2O_4$, $ZnSO_4$, $CaSO_4$, PbS, $PbSO_4$, Pb_3SiO_5, Zn_2SiO_4, ZnS and ZnO. The major phase constituents of the zinc are: $ZnFe_2O_4$ (55.7%), $ZnSO_4$ (22.9%), Zn_2SiO_4 (4.9%) and ZnS(9.4%). The ZnS is in the inner particles with surface wrapped by zinc sulfate, lead sulfate, calcium sulfate and zinc ferrite. The ZLR possesses unstable thermodynamics properties. The water, sulfur trioxide and oxide volatiles escape from the ZLR when temperature is over 200, 700 and 1000 °C, respectively.

2) Leaching toxicity study showed that the amounts of Zn and Cd are 40 and 90 times higher than regulatory limit in a weak acidic environment for short time contact. It is mainly due to the existence of high content of acid exchangeable form of Zn and Cd. A significant amount of Pb and Cu present in the oxidisable form, and this morphology could be changed into acid exchangeable form to bring potential environmental pollution when ZLR is stacked for a long time.

3) The characterization of ZLR using various methods increases the reliability of the results. At the same time, these results provide a more comprehensive view of the possibility to reuse ZLR in other industrial branches to recover metals.

References

[1] ÖZVERDİ A, ERDEM M. Environmental risk assessment and stabilization/solidification of zinc extraction residue: I. Environmental risk assessment [J]. Hydrometallurgy, 2010, 100(3−4): 103−109.

[2] YOUCAI Z, STANFORTH R. Extraction of zinc from zinc ferrites by fusion with caustic soda [J]. Minerals Engineering, 2000, 13(13): 1417−1421.

[3] ALTUNDOĞAN H S, ERDEM M, ORHAN R, OZER A, TUMEN F. Heavy metal pollution potential of zinc leach residues discarded in Cinkur Plant [J]. Turkish Journal of Engineering and Environmental Sciences, 1998, 22(3): 167−177.

[4] TURAN M D, ALTUNDOĞAN H S, TÜMEN F. Recovery of zinc and lead from zinc plant residue [J]. Hydrometallurgy, 2004, 75(1−4): 169−176.

[5] LIU Hong-ping. Surveying the disposal process of zinc leaching slag [J]. Yunnan Metallurgy, 2009, 38(4): 34−38. (in Chinese)

[6] ELGERSMA F, WITKAMP G J, ROSMALEN G M V. Simultaneous dissolution of zinc ferrite and precipitation of ammonium jarosite [J]. Hydrometallurgy, 1993, 34(1): 23−47.

[7] DUTRA A, PAIVA P, TAVARES L. Alkaline leaching of zinc from electric arc furnace steel dust [J]. Minerals Engineering, 2006, 19(5): 478−485.

[8] XIA D K, PICKLES C A. Microwave caustic leaching of electric arc

furnace dust [J]. Minerals Engineering, 2000, 13(1): 79−94.
[9] HOLLOWAY P C, ETSELL T H, MURLAND A L. Roasting of La Oroya zinc ferrite with Na_2CO_3 [J]. Metallurgical and Materials Transactions B, 2007, 38(5): 781−791.
[10] HOLLOWAY P C, ETSELL T H. Recovery of zinc, gallium and indium from La Oroya zinc ferrite using Na_2CO_3 roasting [J]. Mineral Processing and Extractive Metallurgy, 2008, 117(3): 137−146.
[11] MARTINS F M, NETO J M D, CUNHA C J D. Mineral phases of weathered and recent electric arc furnace dust [J]. Journal of Hazardous Materials, 2008, 154(1−3): 417−425.
[12] WEI Y M, SHIMAOKA T, SAFFARZADEH A, TAKAHASHI F. Mineralogical characterization of municipal solid waste incineration bottom ash with an emphasis on heavy metal-bearing phases [J]. Journal of Hazardous Materials, 2011, 187(1−3): 534−543.
[13] US-EPA. Test method for the evaluation of solid waste, physical/chemical methods, Method 1311: Toxicity characteristic leaching procedure [S]. Washington. DC: U. S. Environmental Protection Agency, 1992.
[14] DAVIDSON C M, DUNCAN A L, LITTLEJOHN D, URE A M. A critical evaluation of the three-stage BCR sequential extraction procedure to assess the potential mobility and toxicity of the heavy metals in industrially-contaminated land [J]. Analytica Chimica Acta, 1998, 363(1): 45−55.
[15] GUO Zhao-hui, CHENG Yi, CHAI Li-yuan, SONG Jie. Mineralogical characteristics and environmental availability of non-ferrous slag [J]. Journal of Central South University: Science and Technology, 2007, 38(6): 1100−1105. (in Chinese)
[16] ZHANG Hui-bin. Chemical phase analysis of ore and industrial product [M]. Beijing: Metallurgical Industry Press, 1992. (in Chinese)
[17] MACHADO J G M S, BREHM F A, MORAES C A M, SANTOS C A, VILELA A C F, CUNHA J B M. Chemical, physical, structural and morphological characterization of the electric arc furnace dust [J]. Journal of Hazardous Materials, 2006, 136(3): 953−960
[18] SARGSYAN L Y, HOVHANNISYAN A M. Roasting of the sulfide-zinc concentrate with predominant obtaining of sulfate roast for effective leaching [J]. Russian Journal of Nonferrous Metals, 2010, 51(3): 212−216.
[19] CHOI E J, AHN Y, SONG K C. Mössbauer study in zinc ferrite nanoparticles [J]. Journal of Magnetism and Magnetic Materials, 2006, 301(1): 171−174.
[20] WANG J, WU H Y, YANG C Q, LIN Y L. Room temperature Mössbauer characterization of ferrites with spinel structure [J]. Materials Characterization, 2008, 59 (12): 1716−1720.
[21] CHEN T T, DUTRIZAC J E. Mineralogical changes occurring during the fluid-bed roasting of zinc sulfide concentrates [J]. JOM, 2004, 56(12): 46−51.
[22] BALARINI J C, POLLI L D O, MIRANDA T L S, CASTRO R M Z D, SALUM A. Importance of roasted sulphide concentrates characterization in the hydrometallurgical extraction of zinc [J]. Minerals Engineering, 2008, 21(1): 100−110.
[23] QIAN G R, XU X, SUN W M, XU Y F, LIU Q. Preparation, characterization, and stability of calcium zinc hydrophosphate [J]. Materials Research Bulletin, 2008, 43(12): 3463−3473.
[24] STRASZKO J, OLSZAK-HUMIENIK M, MOZEJKO J. Kinetics of thermal decomposition of $ZnSO_4·7H_2O$ [J]. Thermochimica Acta, 1997, 292(1−2): 145−150.
[25] SIRIWARDANE R V, POSTON J A, FISHER E P, SHEN M S, MILTZ A L. Decomposition of the sulfates of copper, iron(II), iron(III), nickel, and zinc: XPS, SEM, DRIFTS, XRD, and TGA study [J]. Applied Surface Science, 1999, 152(3−4): 219−236.
[26] FROST R L, WEIER M L, MARTENS W. Thermal decomposition of jarosites of potassium, sodium and lead [J]. Journal of Thermal Analysis and Calorimetry, 2005, 82(1): 115−118.
[27] FAN G L, GU Z J, YANG L, LI F. Nanocrystalline zinc ferrite photocatalysts formed using the colloid mill and hydrothermal technique [J]. Chemical Engineering Journal, 2009, 155(1−2): 534−541.
[28] WAGER C D, RIGGS W M, DAVIS L E. Handbook of X-ray photoelectron spectroscopy [M]. Minnesota: Perkin-Emer Corporation, 1979.
[29] GODOČÍKOVÁ E, BASTL Z, SPIROVOVÁ I, BALÁŽ P. A study of mechanochemical reduction of lead sulphide by elemental iron on the surface by X-ray photoelectron spectroscopy [J]. Journal of Materials Science, 2004, 39(9): 3025−3029.
[30] WEN Lu, LIANG Wan-xue, ZHANG Zheng-gang, HUANG Jin-chu. Infrared spectroscopy of minerals [M]. Chongqing: Chongqing University Press, 1988. (in Chinese)
[31] State Environmental Protection Administration of China, GB 5085.3-2007. Hazardous wastes distinction standard-leaching toxicity distinction [S]. Beijing: China Environmental Science Press, 2007. (in Chinese)
[32] RIEUWERTS J S, FARAGO M E, CIKRT M, BENCKO V. Differences in lead bioavailability between a smelting and a mining area [J]. Water, Air and Soil Pollution, 2000, 122(1): 203−229.
[33] MARGUÍ E, QUERALT I, CARVALHO M L, HIDALGO M. Assessment of metal availability to vegetation (Betula pendula) in Pb−Zn ore concentrate residues with different features [J]. Environmental Pollution, 2007, 145(1): 179−184.

锌浸出渣工艺矿物学与环境活性

李 密，彭 兵，柴立元，彭 宁，谢先德，闫 缓

中南大学 冶金科学与工程学院，长沙 410083

摘 要：采用原子吸收光谱(AAS)、X 荧光光谱(XRF)、X 射线衍射(XRD)、穆斯堡尔谱、扫描电镜−能谱(SEM−EDS)、同步热分析仪(TG−DSC)、光电子能谱(XPS)及红外光谱(FTIR)对锌浸出渣的物化性质、物相结构及形貌特征进行研究，采用毒性浸出程序(TCLP)考察锌浸出渣的短期环境活性。物相分析实验结果表明，锌浸出渣的主要组成物相为铁酸锌、硫酸锌和硅酸锌。各种物相以细小的颗粒形式均匀分散在渣中。物化性质分析结果表明，锌浸出渣的热稳定性较差，并且拥有极强的吸水性能。短期 TCLP 分析结果表明，浸出渣中锌和镉不稳定，在弱酸性条件下的浸出率分别超标 40 和 90 倍。

关键词：锌浸出渣；物相组成；微观结构；工艺矿物学；浸出毒性

(Edited by Hua YANG)